



Wear properties of graphene edges probed by atomic force microscopy based lateral manipulation



Borislav Vasić^{a,*}, Aleksandar Matković^{a,1}, Radoš Gajić^a, Igor Stanković^{b,**}

^a Center for Solid State Physics and New Materials, Institute of Physics Belgrade, University of Belgrade, Pregrevica 118, 11080 Belgrade, Serbia

^b Scientific Computing Laboratory, Institute of Physics Belgrade, University of Belgrade, Pregrevica 118, 11080 Belgrade, Serbia

ARTICLE INFO

Article history:

Received 7 April 2016

Received in revised form

15 June 2016

Accepted 19 June 2016

Available online 23 June 2016

ABSTRACT

Excellent elastic properties and good adhesion of graphene to substrate make graphene a promising candidate for application in various friction and wear protective coatings. In order to investigate the response of graphene edges on lateral forces, we combine atomic force microscopy (AFM) based experiments with large scale molecular dynamics (MD) simulations. Exploring movement of AFM tip across graphene edges, we identify four consecutive processes in the course of manipulation: a small increase of lateral force across graphene edges, elastic deformation, plastic deformation followed by permanent wrinkle formation and partial peeling from substrate, and graphene fracture followed by complete peeling within the scan area. In addition, on apexes of graphene flakes, we observe graphene folding followed by the formation of defect free edges. They can prevent further wear to some extent. MD simulations reveal that wrinkles initiated by AFM probe, grow over distance covered by the probe and they are responsible for the observed increase of the lateral force.

© 2016 Elsevier Ltd. All rights reserved.

1. Introduction

Graphene is two-dimensional and atomically thin conductive material with excellent mechanical properties. The Young's modulus of graphene is extremely high, around 1 TPa [1], thus making it the stiffest material known to date, while the friction coefficient is low [2]. At the same time, graphene is very flexible and impermeable to gases supporting the pressure difference of 1 atm [3]. Therefore, graphene can be applied as an extremely compact protective coating for friction and wear reduction [2,4–8], as an anti-corrosion layer [9], for van der Waals screening [10], as a lubricant for rotating and sliding electrical contacts [11], for the mechanical encapsulation and protection of molecules and cells [12–15], and for flexible optoelectronics [16–19].

Atomic force microscope (AFM) is an appropriate tool to study graphene mechanical properties since it allows the measurement of both normal and lateral forces at nanoscale resolution during the

interaction between AFM probe and graphene. AFM based nano-indentation and force-distance measurements were employed to study elastic properties of graphene [1,20–22] and van der Waals screening [10], while frictional properties [23–28] and friction and wear protection [7,29,30] were characterized using the lateral (friction) force microscopy. Strong mechanical interaction between AFM probe and graphene was employed for the graphene patterning based on either static (scratching) [31,32] or dynamic plowing [33].

Behavior of graphene edges subject to lateral forces is also important for the mechanical stability of graphene on a substrate and above mentioned graphene applications. These properties can be studied by AFM probe going across the graphene edges. So far, most of the studies have been devoted to increased sliding friction at step edges of graphite [34–42], MoS₂ [37] and NaCl [37,43] due to a Schwoebel-Ehrlich barrier at steps. The lateral force was applied by AFM probes going across graphene edges in order to study bending properties of functionalized graphene islands [44] and few-layer graphene sheets [45], and to investigate elastic properties of graphene [46] as well as MoS₂ [47] edges. In a similar way, a tribometer was used to measure graphene adhesion by the nano-scratch method [48]. However, wear initiated from graphene edges has not been studied by AFM.

We investigated wear properties of graphene edges by AFM

* Corresponding author.

** Corresponding author.

E-mail addresses: bvasic@ipb.ac.rs (B. Vasić), igor.stankovic@ipb.ac.rs (I. Stanković).

¹ Present address: Institute of Physics, Montanuniversität Leoben, Franz Josef Straße 18, A-8700 Leoben, Austria.

based lateral manipulation both experimentally and using molecular dynamics (MD) simulations. Beside already observed increase of the lateral force at graphite step edges [34–42], we observe and discuss additional structural and mechanical consequences of graphene edge deformation. In addition, we explore apexes of graphene flakes where we observe graphene folding and the formation of defect free edges. We reproduce all elastic features observed in experiment also in MD simulations, and discuss underlying mechanical processes.

2. Methods

2.1. Experimental

Graphene flakes were obtained by micromechanical exfoliation on silicon wafers with a thin layer of silicon-oxide (around 80 nm thick). The flakes were then visualized by optical microscopy, whereas the single layer graphene is confirmed by Raman spectroscopy (see Figs. 1 and 2 in the Supplementary material, respectively).

AFM experiments were performed using NTEGRA Prima system from NT-MDT. Both imaging and AFM manipulations were performed using NSG01 probes from NT-MDT with a typical spring constant 5 N/m and a typical tip curvature radius 6 nm. So far the AFM based lateral manipulation has been used for the controlled movement of three-dimensional nanoparticles [49–55]. AFM manipulation experiments of graphene edges were done in the following way. Initial imaging of graphene flakes was done in the tapping mode. In this mode, the vibrating AFM tip is free from a torsion, so it does not push graphene edges laterally leaving them practically intact. After graphene flakes were found and visualized, AFM manipulations were carried out in the contact mode. Two procedures were applied. In the first one, every image was recorded at the constant normal force, which was then increased in every subsequent scan image. In the second procedure, the normal force was increased after several scan lines within the same scan image. During the AFM manipulations, the lateral deflection of AFM cantilevers was recorded as well. After AFM manipulations, imaging of graphene flakes was done in the tapping mode. All measurements were done at ambient conditions.

2.2. Molecular dynamics simulations

In our atomistic model, a smooth spherical tip with 5 nm radius interacted with graphene sheet edge. The spherical tip is supported by a cylinder of the same radius from the top (see Fig. 3 in the Supplementary material). The SiO₂ substrate had dimensions of 40 × 200 × 5 nm³, whereas the area of the graphene flake was 35 × 190 nm² (the flake was smaller than substrate). The periodic boundaries were set in both directions in the graphene plane (*x* and *y* directions in Fig. 7). Simulation of probe contact and subsequent deformation of graphene sheet are performed with a time step of 0.1 fs and with velocity of 5 m/s. We considered two configurations in MD simulations in which the spherical tip was indented into SiO₂ substrate in the middle of a (1) longer and (2) shorter side of the flake. After that, the tip was moved laterally into the flake. With these two configurations, we were able to investigate wear properties of wide graphene flakes (configuration 1) as well as narrow graphene ribbons and graphene flake apexes (configuration 2). The interatomic forces within SiO₂ and within graphene were derived using appropriate Tersoff potential [56,57]. Adhesion forces between SiO₂ and graphene were modeled with van der Waals potential [58–60], with Lennard-Jones parameters (σ, ϵ) for Si, O and C atoms (0.01301 eV, 3.8264 Å), (0.00650 eV, 3.1181 Å) and (0.00239 eV, 3.4121 Å), respectively. AFM tip was interacting with

the carbon and SiO₂ atoms via purely repulsive shifted Lennard-Jones potential truncated at minimum with the energy parameter $\epsilon = 4$ eV and the repulsion distance $\sigma = 4.5$ Å. The choice of smooth spherical tip and repulsive potential was motivated by a desire to study only influence of adhesion of graphene on substrate and a relatively small contact surface between the AFM tip and graphene. The substrate was supported by a 1 nm layer of SiO₂ atoms connected to their rigid equilibrium position by elastic springs. In the present work, LAMMPS package [61,62] was used for running MD simulations.

3. Results and discussion

Results of AFM manipulation experiments are shown in Fig. 1 for five normal loads: (a) 40 nN, (b) 59 nN, (c) 79 nN, (d) 99 nN, and (e) 118 nN. Topography measured in contact mode during the AFM manipulations is shown in the left column, lateral force (LF) during the scanning in contact mode is shown in the middle column, and topography measured in the tapping mode after the AFM manipulations is shown in the right column. We observe four distinct processes which finally lead to permanent removal of parts of graphene from the surface: (i) a slight increase of lateral force at graphene edge, (ii) elastic strain of graphene edge, (iii) wrinkle formation along graphene edges and partial peeling of graphene from substrate, (iv) graphene fracture and subsequent complete peeling of the graphene flake from the substrate within the scan range during the AFM manipulation.

For all normal loads, there is a slight increase of LF when AFM probe comes into contact with graphene edge. This increase of LF is represented by a dark contrast along graphene edges in the insets of Fig. 1 (a2–d2). The similar, but smaller increase of LF also exists in the backward direction when the probe descends from graphene onto SiO₂ substrate (not shown here). Enhanced LF has been already observed in AFM measurements on graphite [34–42] and graphene [46] step edges due to Schwoebel-Ehrlich barrier. This is an additional barrier for diffusion of surface atom across atomic steps, while in AFM measurements, AFM tip has a role of the surface atom. Still, enhanced LF in the forward direction could originate also from an elastic straining of edge, as it has been already observed in the case of graphene [46] and MoS₂ [47] edges.

At low load, i.e., 40 nN, graphene edge is elastically strained along single scan lines by AFM probe going in the forward direction – from the substrate to graphene. The details of elastic deformation of graphene edge can be seen in the insets of topography in Fig. 1(a1) and LF in Fig. 1(a2). In both insets, graphene surface is bright, but there is a small dark discontinuity around 50 nm long and denoted with the arrow. According to the height and LF profiles for three consecutive scan lines recorded around the observed discontinuity, AFM probe jumps onto graphene at x_1 along line 1. Then, along next line 2, the AFM probe jumps onto graphene at x_2 around 50 nm further away from x_1 . Here the AFM probe pushes graphene edge and signature of graphene deformation is an approximately linear increase of LF seen in the inset of Fig. 1(a2). Then, when AFM probe jumps onto graphene flake, the edge becomes released and returns back into the initial position at x_1 , as can be seen from height and LF profile along line 3. Similar tiny discontinuities in the vicinity of graphene edges are visible in both topography and LF images in Fig. 1(a–d).

For intermediate loads, i.e., 59–99 nN, AFM probe is enough pressed to the surface to avoid graphene slipping. As a result, AFM probe starts to push graphene edge, and forms stable graphene wrinkles. The wrinkles are clearly visible as bright stripes in the topographic images recorded after AFM manipulations (encircled in Fig. 1(b3–d3)). Opposite to the process of elastic straining of graphene edge, the wrinkles are plastic deformations of graphene

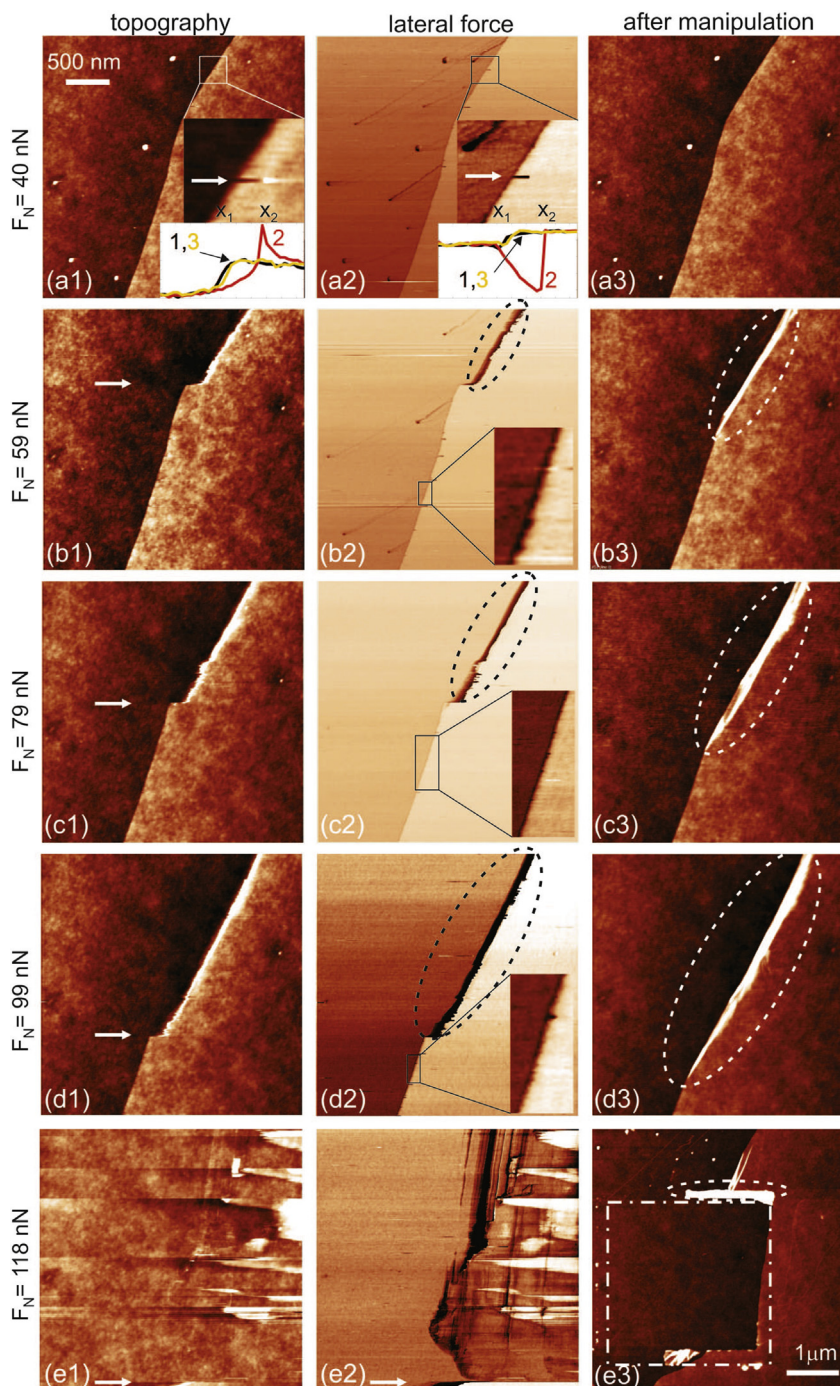


Fig. 1. (a1–e1) Topography and (a2–e2) LF during the AFM manipulation of graphene, and (a3–e3) topography after the manipulation acquired in the tapping mode. (a) Applied normal forces are the following: (a) $F_N = 40$ nN, (b) $F_N = 59$ nN, (c) $F_N = 79$ nN, (d) $F_N = 99$ nN, (e) $F_N = 118$ nN. Elastic deformation of graphene edge and the corresponding change of LF is shown in the insets of parts (a1) and (a2), respectively. Small increase of LF across graphene edge can be seen as a dark contrast in the insets of parts (b2), (c2) and (d2). Arrows in parts (b1), (c1) and (d1) denote the beginning of wrinkle formation. Arrows in parts (e1) and (e2) denote the beginning of graphene tearing. (A colour version of this figure can be viewed online.)

which becomes partially pilled from the substrate. During AFM manipulations, there are sudden and sharp discontinuities both in the topography and LF, as it can be seen in Fig. 1(b1–d1) denoted with arrows and Fig. 1(b2–d2), respectively. Initial peeling of graphene takes place for the first time at these lines and continues up to the end of scan images, meaning that AFM probes subsequently further pushes wrinkled graphene edge. Processes of wrinkle formation and partial peeling of graphene are followed by a significant

increase of LF which is represented by a dark contrast within encircled areas in Fig. 1(b2–d2). Interesting point is that wrinkle bottom is below the corresponding discontinuity denoted with the arrows in Fig. 1(b1–d1). Therefore, when AFM probe hooks graphene edge along the arrows, it pulls also areas of graphene edge which were not deformed when AFM probe went across them.

Results for high loads are given in Fig. 1(e1–e3) (the domain encircled with dashed-dotted line in (e3) corresponds to the

images in (e1) and (e2)). After several initial scan lines at the bottom, graphene is suddenly cut (cuts are denoted with arrows in Fig. 1(e1) and (e2)) and then completely peeled-off within the scan region for AFM manipulation. During the manipulation, the peeled-off part of graphene flake was pulled and/or rolled and finally left at the top part of the scan region where the AFM probe finished the manipulation. This region is visible as a bright stripe in the topography image (encircled domain in Fig. 1(e3)).

Characteristic LF profiles for four processes observed in AFM manipulation of graphene edges are given in Fig. 2. LF is approximately constant when the AFM probe is above either SiO₂ or graphene. On the other hand, when the AFM probe is going across graphene edge, LF grows roughly linearly in all cases. Increase of LF is a result of the peeling of graphene by AFM probe during underlying manipulation process. The resulting structural changes are closely correlated with the LF peak values ΔF_L reached along the distance Δx as denoted in Fig. 2.

Results for the second AFM manipulation experiment are given in Fig. 3. Initial topography is given in Fig. 3(a), while the topography after the manipulation experiment for normal forces $F_N = 59$ nN, $F_N = 79$ nN, and $F_N = 79$ nN, are given in Fig. 3(b),(c),(d), respectively. Similar to the previous example, AFM probe pushes graphene edge and forms wrinkles (encircled in Fig. 3(b) and (c)), while for high enough normal load, this process ends with graphene tearing. Opposite to the previous case, AFM manipulation experiments were stopped (in areas denoted with arrows in Fig. 3(b–d)) after wear was initiated, so graphene is not completely peeled-off from the scan area. We observed again the same four processes characterized with approximately linear increase of LF during AFM manipulations. Fig. 3(c) and (d) were recorded after the manipulations for the same normal load. In Fig. 3(c), graphene edge is only wrinkled, while in Fig. 3(d), this wrinkled edge is cut and further peeled-off from substrate. This is a cumulative effect in a wear of graphene edges since the wear for the same normal load is enhanced for a wrinkled and irregular graphene edge.

Fig. 4 shows distribution of LF peaks ΔF_L versus distance Δx for both manipulation experiments (results from Figs. 1 and 3). The points can be grouped based on process taking place, i.e., into (1) the area of a small LF increase at graphene edge, (2) the area of an elastic deformation of graphene edge, (3) the area of a plastic

deformation of graphene edge, i.e., wrinkle formation, and (4) the area of graphene fracture (graphene cutting and peeling). In the first three areas, graphene edge is in a linear regime where LF approximately linearly increases for a given lateral deformation. Therefore, the graphene edge here behaves as a spring with the effective stiffness $k_{\text{eff}} \approx 0.2$ N/m equal to the slope of the linear fit given by the dashed line in Fig. 4. Distribution of points matches quite well for both experiments in first three areas. Therefore, in both cases graphene edge has approximately the same effective stiffness. We can further derive the following characteristics of graphene edge from areas (1)–(3) in Fig. 4: (i) the maximal LF of around 20 nN for which the graphene edge is in an elastic regime, while for higher forces it starts to deform plastically, and (ii) tensile strength of around 50 nN as maximal LF before graphene tearing and fracture. After tensile stress is reached and graphene fractures, LF depends on amount of graphene fracture by the tip. In both experiments, LF is rather constant and saturates within the fourth area. In the first experiment, graphene was gradually fractured only at the end of every AFM line and pushed to a side, while in the second experiment graphene was fractured continuously with AFM probe movement giving rise to larger LF.

Other AFM manipulation experiments showed that there was no cumulative effect on wear properties of graphene edges only if the applied normal force was below the threshold normal force (below 40 nN). Ten successive scan images for low normal force $F_N = 20$ nN were taken in the contact mode (the results are shown in Fig. 4 in the Supplementary material). As can be seen, there is no wear of graphene edge even after ten cycles. On the other hand, if only a single scan image was recorded at high normal force $F_N = 120$ nN, wear of graphene edge was always initiated (two examples are given in Fig. 5 in the Supplementary material).

In the following AFM manipulation experiments, we focus on wear of graphene edges. In the first case, for intermediate LF, AFM probe pushes graphene edge and form graphene wrinkle, as shown in Fig. 5(a). In the second case, a high LF from AFM probe leads to graphene cutting. This process starts either at contact point between the AFM probe and graphene wrinkle as shown in Fig. 5(b), or at peripheral parts of the wrinkle as shown in Fig. 5(c). All three images were recorded in the tapping mode after the AFM manipulation experiments. All three manipulations were stopped in the regions denoted with arrows in order to avoid complete peeling off graphene within the scan area. This allows us to see shape of graphene after fracture. If AFM probe carried on with scratching of graphene edge, it would hook cut graphene parts. Finally, it would pushed them along virtual paths denoted with dashed arrows in Fig. 5(b) and (c) and left them at the end of the scan range (this would be the top of the scan range since the AFM manipulations were started from the bottom). This mechanism explains shape of graphene after complete peeling given in Fig. 1(e3). Here the encircled part represents exactly the cut graphene piece removed by AFM probe.

Beside wrinkle formation along wide graphene edges, we observed graphene folding as an additional wear mechanism on apexes of graphene flakes. Fig. 6 show two such examples with graphene topography before (the left column) and after (the right column) the AFM manipulation. In the first example shown in Fig. 6(a1) and (a2), AFM probe hooks and lifts encircled apex of graphene flake, folds it (mirror symmetry denoted with M). A subsequent movement of AF probe leads to crumpling of graphene along the top edge. In the second example, we have observed three folding events. Their mirror symmetries are denoted with M_i , $i = 1,2,3$ in Fig. 6(b1) and (b2). As in the previous case, the first folding happens at a very apex of graphene flake which is encircled in Fig. 6(b1). Therefore, graphene folding happens at relatively free edges where the adhesion is the smallest. After the second folding

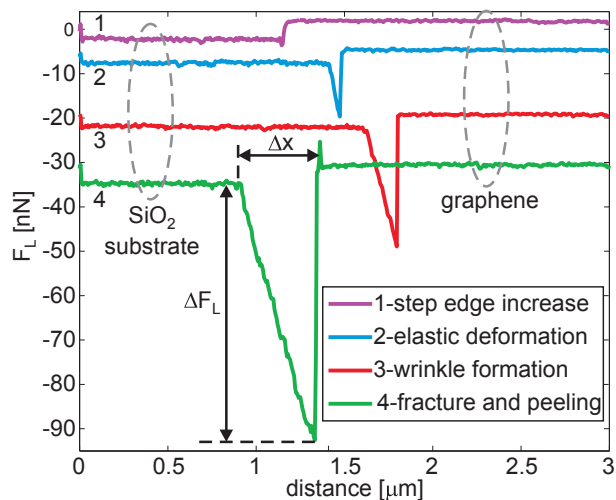


Fig. 2. Change of the lateral force during the observed four regimes: (i) a slight increase of LF at graphene edge, (ii) elastic strain of graphene edge, (iii) wrinkle formation along graphene edges and partial peeling of graphene from substrate, and (iv) graphene fracture. LF cross sections were taken from images in the middle column in Fig. 1. (A colour version of this figure can be viewed online.)

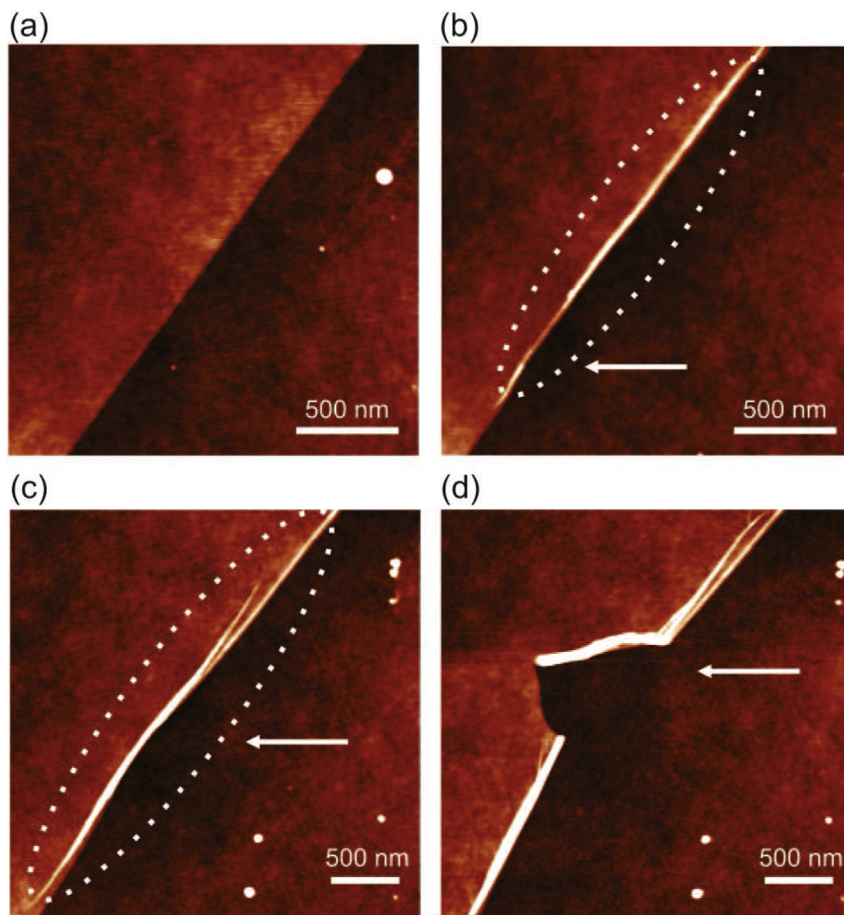


Fig. 3. (a) Initial topography and topography after the AFM manipulation for the following normal forces: (b) $F_N = 59$ nN, (c) $F_N = 79$ nN, and (d) $F_N = 79$ nN. AFM manipulation experiments were stopped along arrows in parts (b), (c) and (d) after wear was initiated. (A colour version of this figure can be viewed online.)

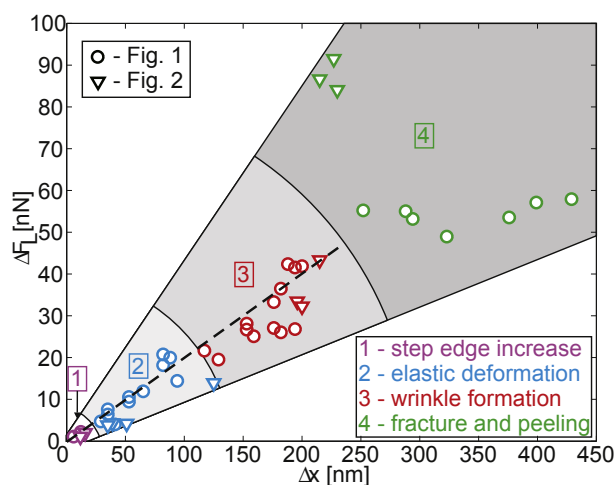


Fig. 4. Distribution of LF peaks ΔF_L versus distance Δx for the results from Fig. 1 (denoted with circles) and Fig. 3 (denoted with triangles). (A colour version of this figure can be viewed online.)

of the graphene flake, a defect free edge of now locally two-layer graphene was formed. The defect free edge in turn prevented further wear of the graphene flake by AFM probe. Therefore, the process of folding of free graphene edges enables inherent prohibition of further wear to some extent. After the third folding, a

region of four-layer graphene is created. It is not flat and the newly formed edge is not regular. For this reason, the graphene folding is followed by cutting of the graphene in the four-layer region (the cut is denoted with the arrow in Fig. 6(b2)).

We used MD simulations in order to reveal and explain fine details in AFM manipulation of graphene edges at atomic scale which can not be resolved by AFM experiments. The simulation results for the manipulation of wide graphene flake with a spherical probe are shown in Fig. 7 (video animations for both top and side view can be found in the Supplementary material). Left (right) panel shows the snapshots of the top (side) view. Graphene is shown in red, while the blue circle denotes the contour of the probe. The probe moves along x-axis and comes across the graphene edge at point A. The probe pushes the edge resulting in the formation of the first graphene wrinkle (point B) which grows with the distance (point C). Further motion of the probe results in the formation (point D) and growing (point E) of the second graphene wrinkle. As a result, the graphene is partially peeled from substrate. When probe pushing graphene edge is removed, the edge is released and it returns back into initial position (snapshots of MD simulation results are given in the Supplementary material in Fig. 6, while video animation for the return of graphene edge in initial position is given in the Supplementary material as well). MD simulation results are in accordance with the experiments: manipulations of graphene edges lead to wrinkle formation with two possibilities, either elastic deformation or plastic with permanent wrinkle formation. At the same time, both experiments and

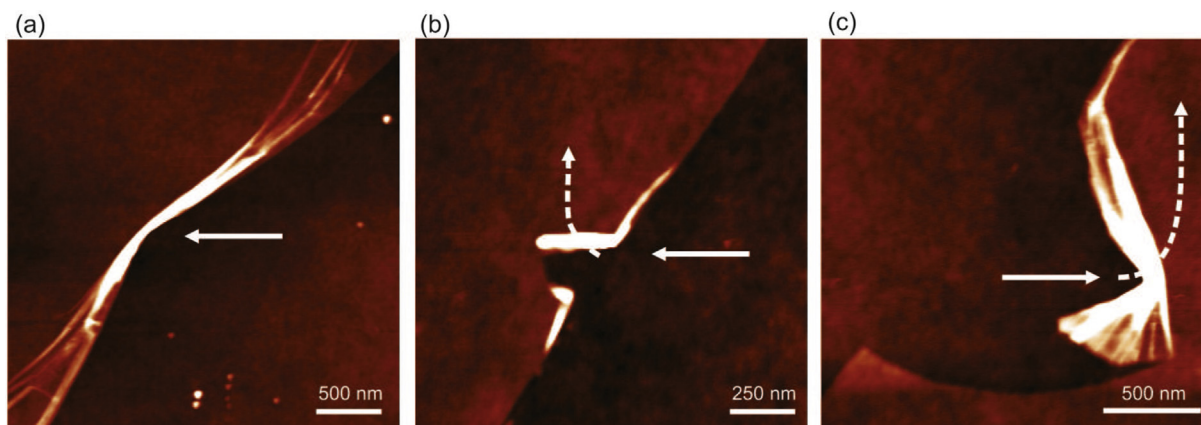


Fig. 5. Wear mechanisms: (a) graphene wrinkle, (b) graphene fracture at contact point between AFM probe and wrinkle, and (c) graphene fracture along peripheral parts of wrinkle. All images were recorded in the tapping mode after AFM manipulations. (A colour version of this figure can be viewed online.)

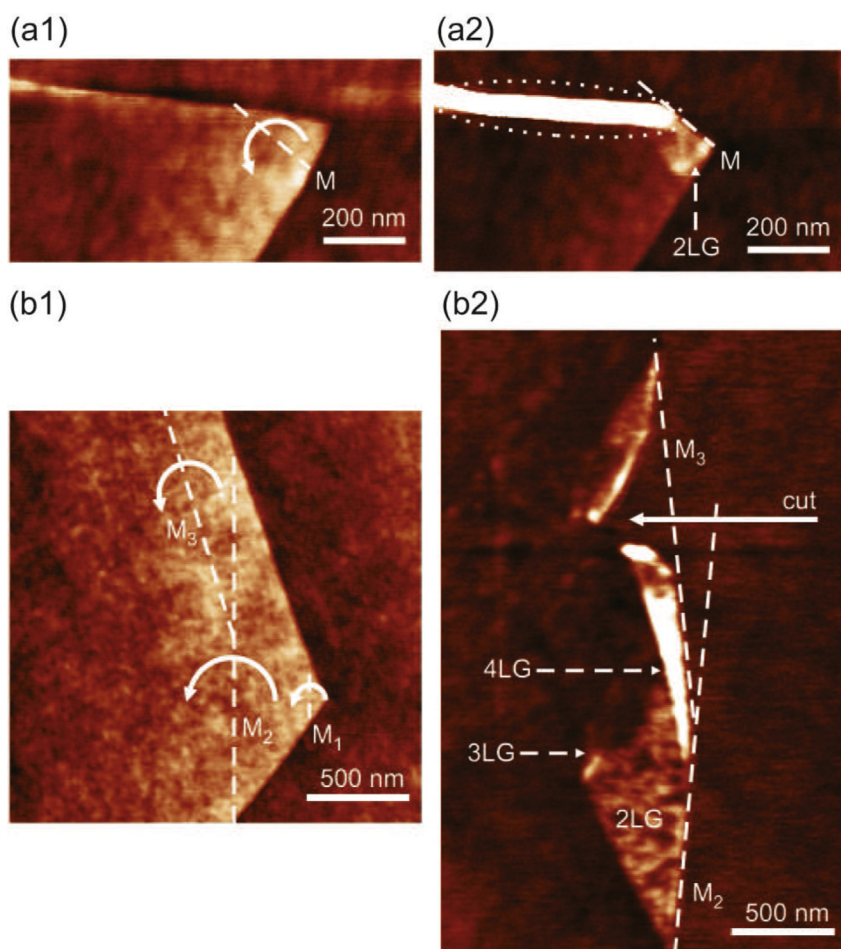


Fig. 6. Folding on apexes of graphene flakes: (a) the case with single fold ((a1) topography before and (a2) after the folding) and (b) the case with three successive folds ((b1) topography before and (b2) after the folding). (A colour version of this figure can be viewed online.)

² Formation of wrinkles was already observed in simulations of sliding of AFM probe on homogeneous graphene sheet, so called the puckering effect [24]. In that case, the normal force from the probe leads to the out-of-plane local deformation of graphene which effectively increase the contact area between the AFM probe and deformed graphene leading to higher friction. When the AFM probe makes indentation of the surface from the side, wrinkles in the graphene sheet are easily formed locally because of the sheet's low bending stiffness compared to its in-plane stiffness. As a result, the graphene sheet is steadily removed from a substrate.

simulations show that the graphene peeling takes place over very wide region on both sides of the probe (for example see Fig. 5(a) and part (E) in Fig. 7).²

Supplementary video related to this article can be found at <http://dx.doi.org/10.1016/j.carbon.2016.06.073>.

MD simulation results for the manipulation of narrow graphene ribbon are shown in Fig. 8 (video animations can be found in the Supplementary material). This case corresponds to the experiments on apexes of graphene flakes (Fig. 6). As can be seen, after AFM

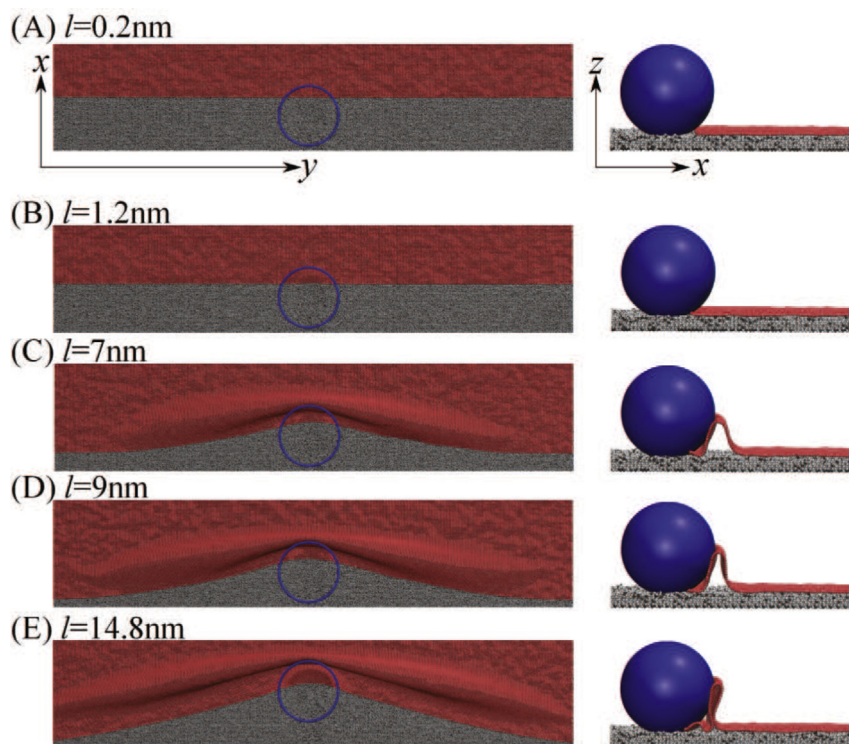


Fig. 7. Snapshots of MD simulation results for the manipulation of graphene edge: snapshots of the top view are shown on the left, while the snapshots for the side view are shown on the right. Distance l covered by the probe is shown on the images. The growth of the first wrinkle can be followed between (B) and (C), and the second smaller wrinkle between (D) and (E). Applied normal force on a bare substrate in the simulations was $F_{N,\text{sub}} = 200$ nN. Only spherical part of the AFM probe is shown, while in our simulations, the sphere is topped by a cylinder of the same radius. (A colour version of this figure can be viewed online.)

probe comes into the contact with graphene edge (point A), it starts to push the edge thus making a wrinkle (points B–D). However, opposite to the case of the wide graphene flake, in this case graphene apex is drawn out and then it is hanging over the rest of the ribbon (point E). Finally, AFM probe would fold released graphene apex, as observed in the experiment.

The simulated evolution of the lateral force exerted on the probe during its movement into the graphene sheet is shown in Fig. 9 (difference $F_L - F_{L,\text{sub}}$ is plotted, where F_L is the total lateral force, whereas $F_{L,\text{sub}}$ is the lateral force on the bare substrate). The

indentation depths in MD simulations were $d_{\text{in}} = 0.3$ nm, 1 nm, 1.5 nm and resulting applied normal forces $F_{N,\text{sub}} = 30$ nN, 150 nN, 200 nN, respectively. Distance of the probe movement is measured from the contact with the graphene. The lateral force depends on applied normal force and distance covered by the probe. For small normal force $F_{N,\text{sub}} = 30$ nN, we observe a steady increase of the lateral force, while graphene flake passes under the tip. After graphene is completely submerged under the probe and when the tip starts just to slide over the graphene, the lateral force saturates.

The higher normal forces ($F_{N,\text{sub}} = 150$ nN, 200 nN) do not

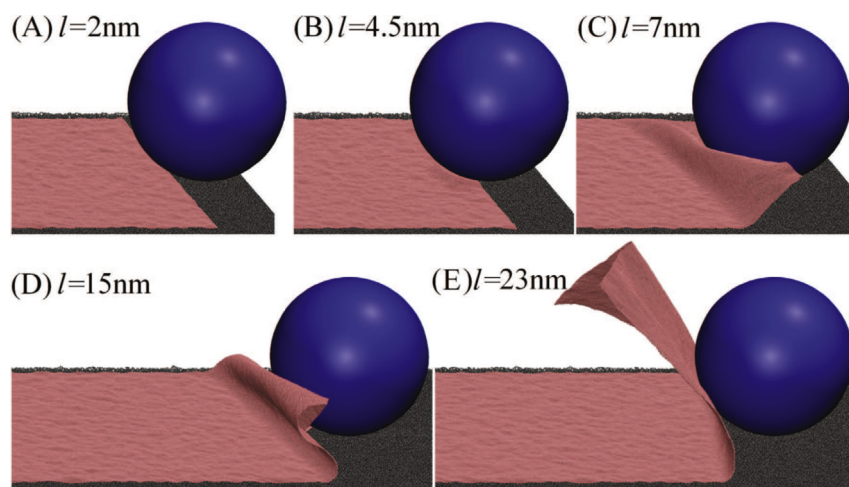


Fig. 8. Snapshots of MD simulation results for the manipulation of graphene ribbon edge as a function of distance l covered by the probe. Applied normal force on a bare substrate in the simulations was $F_{N,\text{sub}} = 200$ nN. Only spherical part of the AFM probe is shown, while in our simulations, the sphere is topped by a cylinder of the same radius. (A colour version of this figure can be viewed online.)

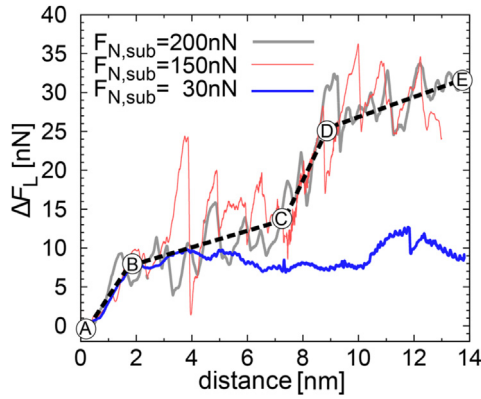


Fig. 9. Change of lateral force $\Delta F_L = F_L - F_{L,sub}$ with displacement of AFM probe, where $F_{L,sub}$ is mean lateral force of bare substrate acting on tip. The results are presented for three initial normal forces of tip on substrate $F_{N,sub} = 30$ nN, 150 nN, 200 nN. Dashed line visualizes changes in slope of lateral force during the slipping of graphene edge under the tip in the regions (A)–(B) and (C)–(D), and the growth of graphene wrinkles in the regions (B)–(C) and (D)–(E). (A colour version of this figure can be viewed online.)

permit graphene to completely slip under the bottom of the tip as can be seen in Fig. 7. From point A to point B in Fig. 7, the graphene edge is a physical obstacle for the probe and it exerts a force in the lateral direction on the tip. The graphene penetrates only up to certain depth under the tip and then pulls out (point B). As result we first observe growth of one wrinkle (B to C), i.e., out-of-plane deformation of graphene sheet, and then with increasing distance the second wrinkle forms and grows (from point D to point E). These wrinkles result in a step-wise increase of the lateral force as can be seen in Fig. 9. The height of the first step of the lateral force ΔF_L has the same value as in the case of tip sliding on top of the graphene. This indicates that a source of the first step of lateral force is just the graphene sandwiched between the tip and substrate in direction of the movement. The growth of the wrinkles is limited by curvature of the tip. When a wrinkle touches the tip, we observe a further stepwise increase in the lateral force.

We have performed additional MD simulations in which a probe was moving under the angles 45° , 60° , 75° relative to graphene edge, and then compared these results with the probe moving orthogonally under 90° angle. The configurations where probe is moving oblique to graphene edge are typically seen in experiment. From dynamical point of view, the movement of the probe oblique to the edge involves steady shear of graphene flake between the probe and substrate. The evolution of LF with displacement of the probe is shown in Fig. 10. One can immediately observe a steady increase of lateral force for 45° and 60° (upper panel). The side motion and shear prevent slipping of the graphene between AFM tip and substrate and step-wise increase of the lateral force which on the other hand grows continuously for these configurations. The slope of LF increase is similar in both cases and roughly 1 N/m. The slope of LF in the experiment (e.g. in Fig. 4) is about 0.2 N/m. The reason for discrepancy could be absence of a water layer between graphene and silicon oxide substrate in our simulations, therefore overestimating adhesion compared to experiment. When side motion is smaller, the lateral force starts to build up stepwise as can be seen in bottom panel in Fig. 10 for 75° angle, and which is reminiscent of the case when probe is moving orthogonally for 90° angle when the stepwise increase is obvious.

MD simulations allow us to get insights into energy landscape changes during the manipulation of graphene edges. In the conclusion of the results section, we would like therefore to discuss evolution of intra graphene energy (covalent C–C bonds, see 11(a))

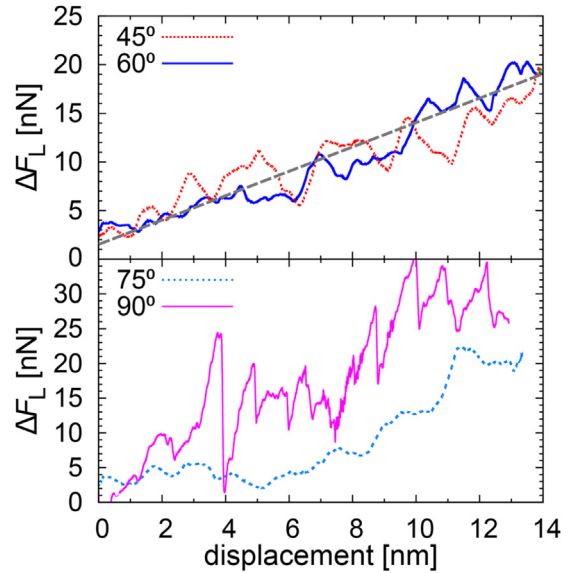


Fig. 10. The evolution of LF with displacement of AFM probe moving under the angles 45° , 60° , 75° , 90° relative to graphene edge and initially applied normal forces of tip on substrate was $F_{N,sub} = 150$ nN. Dashed line in the top panel is guide to the eye emphasizing the linear increase and the similar slope of the lateral force for both angles. (A colour version of this figure can be viewed online.)

with deformation caused by tip in the linear regime (before fracture). The work by AFM probe is used for partial graphene peeling countering van der Waals forces between graphene and substrate, and graphene deformation. The total energy increase in graphene ΔE_{CC} (energy of all C–C bonds) is given in Fig. 11(a). ΔE_{CC} starts to grow significantly after the distance of around 7 nm. This distance corresponds to the point where second wrinkle starts to form and lateral force increases beyond lateral force of tip shearing over the graphene (cf. Fig. 9 between points (C) and (D)). Therefore, graphene wrinkles touching and pushing the tip lead to the increase of the elastic energy. Change of the local graphene energy Δe_{CC} , which corresponds to the energy of C–C bonds of each graphene atom, is given in Fig. 11(b). The increase of energy of carbon atoms is largest in the vicinity of the AFM probe and reaches 40 meV per atom after the probe has covered 14 nm. At the same time, change of the adhesion energy between graphene and SiO_2 substrate is $\gamma_{adh} \Delta x L / 2 \approx 2$ keV, where $\gamma_{adh} = 0.45 \text{ Jm}^{-2}$ is the adhesion energy of graphene on silicon oxide substrate [63], $\Delta x = 14$ nm is the distance covered by AFM probe, and $L = 100$ nm is the size of the triangular patch with bare silicon dioxide substrate left after graphene peeling. Change of the adhesion energy is larger than the energy of graphene deformation $\Delta E_{CC} \approx 1$ keV after $\Delta x = 14$ nm meaning that a greater part of the work done by the probe is used to overcome graphene-substrate adhesion.

4. Conclusion

We studied wear of graphene edges as the departure point of the global wear of graphene coating. Its edges governed in this frame wear resistivity of various graphene based protective coatings. Wear of graphene edges started with wrinkle formation. High enough normal loads resulted in their fracture at points of largest elastic energy, and subsequent peeling of graphene from substrate. Wear was enhanced on irregular and already wrinkled graphene edges. On the other hand, graphene flakes still have the ability to prevent and stop damage from spreading in the case of folding when new and regular edges are formed. Deformation of graphene

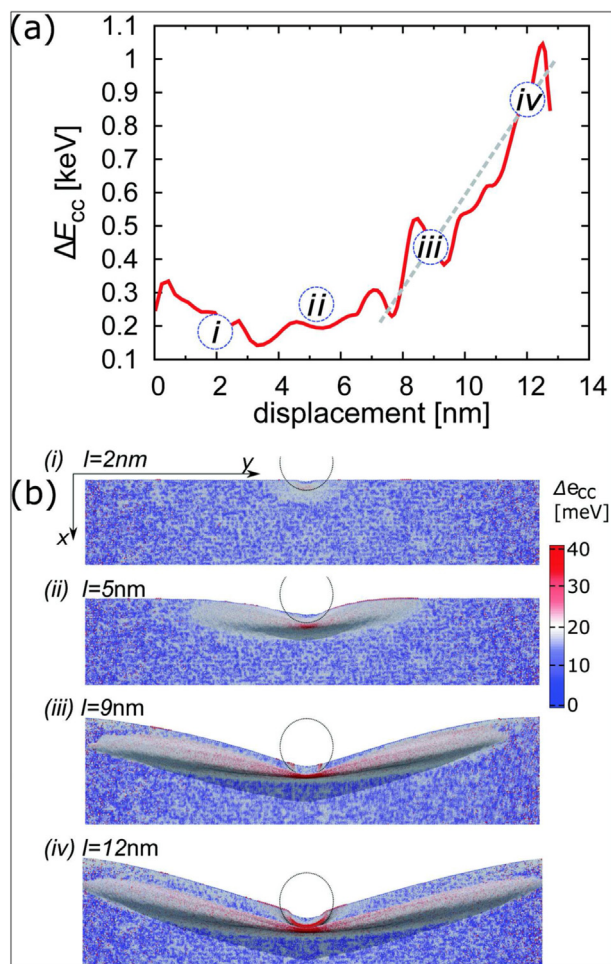


Fig. 11. Change of (a) total intra graphene energy ΔE_{cc} and (b) local energy Δe_{cc} of each graphene atom (only covalent C–C bond energy). The dashed line on the plot is a guide to the eye and shows trend of energy increase. The configurations (i) and (ii) correspond to the first wrinkle growth, configuration (iii) is after the second wrinkle formation and steep lateral force increase, and (iv) corresponds to the growth of the second wrinkle. (A colour version of this figure can be viewed online.)

edges was followed by increasing lateral force due to wrinkle formation and an increased contact area between AFM probe and graphene edge. The major work done by AFM probe was used to overcome adhesion energy. Therefore, wear of graphene edges could be decreased in the case of larger graphene-substrate adhesion, e.g. by removal of water layer.

Our results indicate that the normal force acting on AFM tip and the graphene edge structure were two principal factors which determined wear behavior of the graphene edge. The complete wear of a defect free edge started only for a sufficiently large normal force. This can be rationalized from the MD simulation results. We observe that the AFM based lateral manipulation of graphene edge results in wrinkle formation. When AFM tip started to slide over the graphene flake, the adhesion would either flatten graphene edge covering substrate again, or if deformation progressed beyond a threshold value, stable wrinkle was formed. In the later case, graphene was partially peeled-off from substrate.

This study also showed that AFM could be very useful for the mechanical manipulation of a truly two-dimensional nano-objects and materials. The method presented here could be used to study interaction between adjacent layers in multi-layer two-dimensional materials of for surface peeling in order to make novel and

hybrid surfaces [64–66].

This work is supported by the Serbian Ministry of Education, Science and Technological Development under Project No. OI171005, OI171017, and III45018, and in part by COST Action MP1303. Numerical simulations were run on the PARADOX supercomputing facility at the Scientific Computing Laboratory of the Institute of Physics Belgrade. The authors would like to acknowledge Uroš Ralević for help with Raman measurements of graphene samples.

Appendix A. Supplementary data

Supplementary data related to this article can be found at <http://dx.doi.org/10.1016/j.carbon.2016.06.073>.

References

- [1] C. Lee, X. Wei, J.W. Kysar, J. Hone, Measurement of the elastic properties and intrinsic strength of monolayer graphene, *Science* 321 (2008) 385–388.
- [2] K.-S. Kim, H.-J. Lee, C. Lee, S.-K. Lee, H. Jang, J.-H. Ahn, et al., Chemical vapor deposition-grown graphene: the thinnest solid lubricant, *ACS Nano* 5 (2011) 5107–5114.
- [3] J.S. Bunch, S.S. Verbridge, J.S. Alden, A.M. van der Zande, J.M. Parpia, H.G. Craighead, et al., Impermeable atomic membranes from graphene sheets, *Nano Lett.* 8 (2008) 2458–2462.
- [4] D. Berman, A. Erdemir, A.V. Sumant, Graphene: a new emerging lubricant, *Mater. Today* 17 (2014) 31–42.
- [5] D. Marchetto, C. Held, F. Hausen, F. Wühlisch, M. Dienwiebel, R. Bennewitz, Friction and wear on single-layer epitaxial graphene in multi-asperity contacts, *Tribol. Lett.* 48 (2012) 77–82.
- [6] F. Wühlisch, J. Hoth, C. Held, T. Seyller, R. Bennewitz, Friction and atomic-layer-scale wear of graphitic lubricants on SiC(0001) in dry sliding, *Wear* 300 (2013) 78–81.
- [7] A. Klemenz, L. Pastewka, S.G. Balakrishna, A. Caron, R. Bennewitz, M. Moseler, Atomic scale mechanisms of friction reduction and wear protection by graphene, *Nano Lett.* 14 (2014) 7145–7152.
- [8] D. Berma, A. Erdemir, A.V. Sumant, Few layer graphene to reduce wear and friction on sliding steel surfaces, *Carbon* 54 (2013) 454–459.
- [9] N.T. Kirkland, T. Schiller, N. Medhekar, N. Birbilis, Exploring graphene as a corrosion protection barrier, *Corros. Sci.* 56 (2012) 1–4.
- [10] S. Tsoi, P. Dev, A.L. Friedman, R. Stine, J.T. Robinson, T. Reinecke, et al., Van der Waals screening by single-layer graphene and molybdenum disulfide, *ACS Nano* 8 (2014) 12410–12417.
- [11] D. Berman, A. Erdemir, A.V. Sumant, Graphene as a protective coating and superior lubricant for electrical contacts, *Appl. Phys. Lett.* 105 (2014) 231907.
- [12] N. Severin, M. Dorn, A. Kalachev, J.P. Rabe, Replication of single macromolecules with graphene, *Nano Lett.* 11 (2011) 2436–2439.
- [13] N. Mohanty, M. Fahrenholtz, A. Nagaraja, D. Boyle, V. Berry, Impermeable graphenic encasement of bacteria, *Nano Lett.* 11 (2011) 1270–1275.
- [14] R. Kempaiah, S. Salgado, W.L. Chung, V. Maheshwari, Graphene as membrane for encapsulation of yeast cells: protective and electrically conducting, *Chem. Commun.* 47 (2011) 11480–11482.
- [15] A. Matković, B. Vasić, J. Pešić, J. Prinz, I. Bald, R. Milosavljević, A. Gajić, Enhanced structural stability of DNA origami nanostructures by graphene encapsulation, *New J. Phys.* 18 (2016) 025016.
- [16] K.S. Kim, Y. Zhao, H. Jang, S.Y. Lee, J.M. Kim, K.S. Kim, et al., Large-scale pattern growth of graphene films for stretchable transparent electrodes, *Nature* 457 (2009) 706–710.
- [17] L. Gomez De Arco, Y. Zhang, C.W. Schlenker, K. Ryu, M.E. Thompson, C. Zhou, Continuous, highly flexible, and transparent graphene films by chemical vapor deposition for organic photovoltaics, *ACS Nano* 4 (2010) 2865–2873.
- [18] M. Kratzer, S. Klima, C. Teichert, B. Vasić, A. Matković, U. Ralević, et al., Temperature dependent growth morphologies of parahexaphenyl on SiO₂ supported exfoliated graphene, *J. Vac. Sci. Technol. B* 31 (2013) 04.
- [19] K. Rana, J. Singh, J.-H. Ahn, A graphene-based transparent electrode for use in flexible optoelectronic devices, *J. Mater. Chem. C* 2 (2014) 2646–2656.
- [20] C.S. Ruiz-Vargas, H.L. Zhuang, P.Y. Huang, A.M. van der Zande, S. Garg, P.L. McEuen, et al., Softened elastic response and unzipping in chemical vapor deposition graphene membranes, *Nano Lett.* 11 (2011) 2259–2263.
- [21] G.-H. Lee, R.C. Cooper, S.J. An, S. Lee, A. van der Zande, N. Petrone, et al., High-strength chemical-vapor-deposited graphene and grain boundaries, *Science* 340 (2013) 1073–1076.
- [22] H.I. Rasool, C. Ophus, W.S. Klug, A. Zettl, J.K. Gimzewski, Measurement of the intrinsic strength of crystalline and polycrystalline graphene, *Nat. Commun.* 4 (2013) 2811.
- [23] T. Filleter, J.L. McChesney, A. Bostwick, E. Rotenberg, K.V. Emtsev, T. Seyller, et al., Friction and dissipation in epitaxial graphene films, *Phys. Rev. Lett.* 102 (2009) 086102.
- [24] C. Lee, Q. Li, W. Kalb, X.-Z. Liu, H. Berger, R.W. Carpick, et al., Frictional characteristics of atomically thin sheets, *Science* 328 (2010) 76–80.

- [25] H. Lee, N. Lee, Y. Seo, J. Eom, S. Lee, Comparison of frictional forces on graphene and graphite, *Nanotechnology* 20 (2009) 325701.
- [26] S. Kwon, J.-H. Ko, K.-J. Jeon, Y.-H. Kim, J.Y. Park, Enhanced nanoscale friction on fluorinated graphene, *Nano Lett.* 12 (2012) 6043–6048.
- [27] G. Fessler, B. Eren, U. Gysin, T. Glatzel, E. Meyer, Friction force microscopy studies on SiO₂ supported pristine and hydrogenated graphene, *Appl. Phys. Lett.* 104 (2014) 041910.
- [28] H. Chen, T. Filleter, Effect of structure on the tribology of ultrathin graphene and graphene oxide films, *Nanotechnology* 26 (2015) 135702.
- [29] L.-Y. Lin, D.-E. Kim, W.-K. Kim, S.-C. Jun, Friction and wear characteristics of multi-layer graphene films investigated by atomic force microscopy, *Surf. Coat. Technol.* 205 (2011) 4864–4869.
- [30] B. Vasić, A. Zurutuza, R. Gajić, Spatial variation of wear and electrical properties across wrinkles in chemical vapour deposition graphene, *Carbon* 102 (2016) 304–310.
- [31] A.J.M. Giesbers, U. Zeitler, S. Neubeck, F. Freitag, K.S. Novoselov, J.C. Maan, Nanolithography and manipulation of graphene using an atomic force microscope, *Solid State Commun.* 147 (2008) 366–369.
- [32] S. Eilers, J.P. Rabe, Manipulation of graphene within a scanning force microscope, *Phys. Status Solidi B* 246 (2009) 2527–2529.
- [33] B. Vasić, M. Kratzer, A. Matković, A. Nevesad, U. Ralević, D. Jovanović, et al., Atomic force microscopy based manipulation of graphene using dynamic plowing lithography, *Nanotechnology* 24 (2013) 015303.
- [34] J. Ruan, B. Bhushan, Frictional behavior of highly oriented pyrolytic graphite, *J. Appl. Phys.* 76 (1994) 8117–8120.
- [35] E. Meyer, R. Lüthi, L. Howald, M. Bammerlin, M. Guggisberg, H.J. Güntherodt, Site-specific friction force spectroscopy, *J. Vac. Sci. Technol. B* 14 (2) (1996) 1285–1288.
- [36] T. Müller, M. Lohrmann, T. Kässer, O. Marti, J. Mlynek, G. Krausch, Frictional force between a sharp asperity and a surface step, *Phys. Rev. Lett.* 79 (1997) 5066–5069.
- [37] H. Hölscher, D. Ebeling, U.D. Schwarz, Friction at atomic-scale surface steps: experiment and theory, *Phys. Rev. Lett.* 101 (2008) 246105.
- [38] Y. Dong, X.Z. Liu, P. Egberts, Z. Ye, R.W. Carpick, A. Martini, Correlation between probe shape and atomic friction peaks at graphite step edges, *Tribol. Lett.* 50 (2012) 49–57.
- [39] P. Egberts, Z. Ye, X.Z. Liu, Y. Dong, A. Martini, R.W. Carpick, Environmental dependence of atomic-scale friction at graphite surface steps, *Phys. Rev. B* 88 (2013) 035409.
- [40] Z. Ye, A. Otero-de-la Roza, E.R. Johnson, A. Martini, Effect of tip shape on atomic-friction at graphite step edges, *Appl. Phys. Lett.* 103 (2013) 081601.
- [41] H. Lee, H.-B.-R. Lee, S. Kwon, M. Salmeron, J.Y. Park, Internal and external atomic steps in graphite exhibit dramatically different physical and chemical properties, *ACS Nano* 9 (2015) 3814–3819.
- [42] Z. Ye, A. Martini, Atomic friction at exposed and buried graphite step edges: experiments and simulations, *Appl. Phys. Lett.* 106 (2015) 231603.
- [43] P. Steiner, E. Gnecco, F. Krok, J. Budzioch, L. Walczak, J. Konior, et al., Atomic-scale friction on stepped surfaces of ionic crystals, *Phys. Rev. Lett.* 106 (2011) 186104.
- [44] H.C. Schniepp, K.N. Kudin, J.-L. Li, R.K. Prud'homme, R. Car, D.A. Saville, I.A. Aksay, Bending properties of single functionalized graphene sheets probed by atomic force microscopy, *ACS Nano* 2 (2008) 2577–2584.
- [45] X. Chen, C. Yi, C. Ke, Bending stiffness and interlayer shear modulus of few-layer graphene, *Appl. Phys. Lett.* 106 (2015) 101907.
- [46] D.P. Hunley, T.J. Flynn, T. Dodson, A. Sundararajan, M.J. Boland, D.R. Strachan, Friction, adhesion, and elasticity of graphene edges, *Phys. Rev. B* 87 (2013) 035417.
- [47] M.J. Boland, M. Nasser, D.P. Hunley, A. Ansary, D.R. Strachan, Striped nanoscale friction and edge rigidity of MoS₂ layers, *RSC Adv.* 5 (2015) 92165–92173.
- [48] S. Das, D. Lahiri, A. Agarwal, W. Choi, Interfacial bonding characteristics between graphene and dielectric substrates, *Nanotechnology* 25 (2014) 045707.
- [49] T. Junno, K. Deppert, L. Montelius, L. Samuelson, Controlled manipulation of nanoparticles with an atomic force microscope, *Appl. Phys. Lett.* 66 (1995) 3627–3629.
- [50] L. Theil Hansen, A. Kühle, A.H. Sørensen, J. Bohr, P.E. Lindelof, A technique for positioning nanoparticles using an atomic force microscope, *Nanotechnology* 9 (1998) 337.
- [51] C. Ritter, M. Heyde, U.D. Schwarz, K. Rademann, Controlled translational manipulation of small latex spheres by dynamic force microscopy, *Langmuir* 18 (2002) 7798–7803.
- [52] D. Dietzel, T. Mönninghoff, L. Jansen, H. Fuchs, C. Ritter, U.D. Schwarz, et al., Interfacial friction obtained by lateral manipulation of nanoparticles using atomic force microscopy techniques, *J. Appl. Phys.* 102 (2007) 084306.
- [53] D. Dietzel, C. Ritter, T. Mönninghoff, H. Fuchs, A. Schirmeisen, U.D. Schwarz, Frictional duality observed during nanoparticle sliding, *Phys. Rev. Lett.* 101 (2008) 125505.
- [54] K. Mougín, E. Gnecco, A. Rao, M.T. Cuberes, S. Jayaraman, E.W. McFarland, et al., Manipulation of gold nanoparticles: influence of surface chemistry, temperature, and environment (vacuum versus ambient atmosphere), *Langmuir* 24 (2008) 1577–1581.
- [55] D. Dietzel, U.D. Schwarz, A. Schirmeisen, Nanotribological studies using nanoparticle manipulation: principles and application to structural lubricity, *Friction* 2 (2014) 114–139.
- [56] J. Tersoff, New empirical approach for the structure and energy of covalent systems, *Phys. Rev. B* 37 (1988) 6991–7000.
- [57] J. Tersoff, Modeling solid-state chemistry: interatomic potentials for multi-component systems, *Phys. Rev. B* 39 (1989) 5566–5568.
- [58] E.P. Bellido, J.M. Seminario, Molecular dynamics simulations of folding of supported graphene, *J. Phys. Chem. C* 114 (2010) 22472–22477.
- [59] E. Paek, G.S. Hwang, A computational analysis of graphene adhesion on amorphous silica, *J. Appl. Phys.* 113 (2013) 164901.
- [60] W. Gao, P. Xiao, G. Henkelman, K.M. Liechti, R. Huang, Interfacial adhesion between graphene and silicon dioxide by density functional theory with van der Waals corrections, *J. Phys. D Appl. Phys.* 47 (2014) 255301.
- [61] <http://lammmps.sandia.gov/index.html>.
- [62] S. Plimpton, Fast parallel algorithms for short-range molecular dynamics, *J. Comput. Phys.* 117 (1995) 1–19.
- [63] S.P. Koenig, N.G. Boddeti, M.L. Dunn, J.S. Bunch, Ultrastrong adhesion of graphene membranes, *Nat. Nano* 6 (2011) 543–546.
- [64] S.S. Hong, W. Kundhikanjana, J.J. Cha, K. Lai, D. Kong, S. Meister, et al., Ultrathin topological insulator Bi₂Se₃ nanoribbons exfoliated by atomic force microscopy, *Nano Lett.* 10 (2010) 3118–3122.
- [65] P. Seema, J. Behler, D. Marx, Peeling by nanomechanical forces: a route to selective creation of surface structures, *Phys. Rev. Lett.* 115 (2015) 036102.
- [66] T. Korhonen, P. Koskinen, Peeling of multilayer graphene creates complex interlayer sliding patterns, *Phys. Rev. B* 92 (2015) 115427.